A transcriptomics-guided drug target discovery strategy identifies novel receptor ligands for lung regeneration

Xinhui Wu[1,2], I. Sophie T. Bos[1,2], Thomas M. Conlon[3], Meshal Ansari[3], Vicky Verschut[1,6] Lars A. Verkleij[1,2], Angela D'Ambrosi[1,2], Aleksey Matveyenko[4], Herbert B. Schiller[3], Melanie Königshoff[5], Martina Schmidt[1,2], Loes E. M. Kistemaker[1,2,6], Ali Önder Yildirim[3], Reinoud Gosens[1,2, *]

[1]Department of Molecular Pharmacology, Faculty of Science and Engineering, University of Groningen, Antonius Deusinglaan 1, 9713AV, Groningen, The Netherlands, [2]Groningen Research Institute for Asthma and COPD, University Medical Center Groningen, University of Groningen, Groningen, The Netherlands, [3]Institute of Lung Biology and Disease (ILBD)/Comprehensive Pneumology Center (CPC), Helmholz Zentrum München, Munich, Germany, Member of the German Center for Lung Research (DZL), [4]Department of Physiology and Biomedical Engineering, Mayo Clinic Collage of Medicine, Rochester, Minnesota, USA, [5]University of Pittsburg, [6]Aquilo BV, Groningen, The Netherlands, *Correspondence

19 **Abstract**

20 Currently, there is no pharmacological treatment targeting defective tissue repair in

21 chronic disease. Here we utilized a transcriptomics-guided drug target discovery

22 strategy using gene signatures of smoking-associated chronic obstructive pulmonary

23 disease (COPD) and from mice chronically exposed to cigarette smoke, identifying

24 druggable targets expressed in alveolar epithelial progenitors of which we screened

25 the function in lung organoids. We found several drug targets with regenerative

26 potential of which EP and IP prostanoid receptor ligands had the most significant

27 therapeutic potential in restoring cigarette smoke-induced defects in alveolar epithelial

28 progenitors *in vitro* and *in vivo*. Mechanistically, we discovered by using scRNA-

29 sequencing analysis that circadian clock and cell cycle/apoptosis signaling pathways

30 were enriched in alveolar epithelial progenitor cells in COPD patients and in a relevant

31 model of COPD, which was prevented by PGE2 or PGI2 mimetics. Conclusively,

32 specific targeting of EP and IP receptors offers therapeutic potential for injury to repair

33 in COPD.

34

35 **Key words:** PGE2; PGI2; repair; cell cycle; circadian clock signaling; drug screening

36

37

38

Introduction

One of the main challenges in pharmacology today is the generation of drugs with regenerative potential, with the ability to restore tissue repair in chronic disease. Regenerative medicine has thus far mainly focused on transplantation, tissue engineering approaches, stem- or progenitor cell therapy, or a combination of these[1]. A regenerative pharmacological approach will have considerable additional potential because it can be applied on a relatively large scale. Furthermore, it can be used to halt the disease process in an early stage resulting in real disease-modifying treatment. Also, pharmacological targeting may aid or support other regenerative strategies.

There is a need for regenerative pharmacology in respiratory, cardiovascular, and neurological diseases as well as many other disease areas. In respiratory medicine, chronic obstructive pulmonary disease (COPD) is one of the most common lung diseases with a need for regenerative therapies. The disease is characterized by airflow limitation that is not fully reversible, and which deteriorates progressively. The main difficulty underlying COPD pathogenesis is increased tissue destruction in combination with abnormal tissue repair in susceptible individuals. As current therapies do not modify the course of the disease, developing new therapeutic strategies aiming at regeneration of tissue is necessary.

In affected individuals, there is an increase in alveolar air space associated with destruction of alveolar epithelial cells along with reduced capacity of epithelial progenitors to restore this defect. In the distal lung, alveolar type II cells and alveolar epithelial progenitors harbour stem cell capacity and function to maintain alveolar epithelium[2]. These cells reside in a local tissue microenvironment called the niche, which is composed of supporting cells such as fibroblasts and alveolar macrophages. The niche controls adequate activation of the progenitor cell[1–3] by means of secreted

64 factors such as WNTs, FGFs, retinoic acid, and many other factors that control

65 stemness, proliferation and differentiation[3].

66 Like in many chronic diseases associated with ageing, this local lung

67 microenvironment is insufficiently supportive for lung repair in COPD [1,4,5]. For example,

68 studies have indicated that an imbalance of canonical and noncanonical WNT

69 signaling results in impaired alveolar regeneration in COPD[4,6]. Moreover, lymphotoxin-

70 β (LTβ), released from CD8+ T-cells in COPD, can negatively interfere with repair.

71 LTβ induces noncanonical NFκB signalling, thereby repressing functional Wnt/β-

72 catenin signalling in the lung[5]. Accordingly, the challenge towards successful

73 regenerative pharmacology in COPD needs to take into consideration the specific

74 hostile microenvironment and the abnormal repair process that stands in the way of

75 adequate regeneration in COPD.

76 In the present study, we hypothesized that a transcriptomics guided drug target

77 discovery strategy based on gene signatures differentially expressed in COPD and in

78 response to cigarette smoke may be used to identify novel druggable gene targets

79 that are specifically involved in defective lung repair in COPD. Our results show that

80 such a strategy coupled to functional studies in organoids yields novel receptor ligands

81 of which EP and IP prostanoid receptor had the most significant potential in

82 counteracting the negative effects of cigarette smoke on alveolar progenitor cell

83 function.

84 **Results**

85 **Transcriptomics-guided screening to identify novel targets.** We set out to identify

86 novel drug targets that may help restore defective lung repair. To achieve this, we

87 utilized a transcriptomics-guided target discovery strategy (described in Fig. 1a) based

88 on gene signatures of COPD lung tissues [7] and of a relevant model of cigarette smoke

89 exposure[8] to identify differentially regulated druggable genes. We found Reactome

90 pathways related to inflammation such as *Neutrophil degranulation* and *Innate*

91 *immune system* as well as pathways related to the extracellular matrix such as

92 *Extracellular matrix organization* and *Integrin cell surface interactions* to be enriched

93 in both datasets (Fig. 1b-e). We identified 38 individual target genes that were

94 concordantly up- and 30 individual target genes concordantly downregulated. These

95 genes were filtered through the 'Drug-gene interactions and potential druggability in

96 the drug gene interaction database' (DGIdb, http://www.dgidb.org/), which rendered

97 25 druggable upregulated genes and 16 druggable downregulated genes (Fig. 1f).

98 Genes were further filtered for expression in lung epithelial cells or fibroblasts by

99 consulting the human lung cell atlas (https://asthma.cellgeni.sanger.ac.uk/) and lung

100 map (https://lungmap.net/), which yielded 15 druggable target genes.

101

Figure 1 Overview of the transcriptomics-guided drug discovery strategy. a Schematic outline of the drug screening strategy. **b-c** Reactome pathway enrichment analysis of differentially up- and downregulated genes from CS-exposed mice[8] using GSEA (https://www.gsea-msigdb.org/gsea/msigdb/annotate.jsp). **d-e** Reactome pathway enrichment analysis of up- and

106   downregulated genes from COPD patients[7] using GSEA, the top 20 pathways enriched are presented.

107   **f** Heatmap shows the gene expression pattern of the druggable genes (http://www.dgidb.org/) identified

108   both in CS-exposed mice and COPD patient databases.

109   To assess the potential relevance of signaling functionally associated with the 15

110   genes of interest, we set up an *in vitro* organoid model to perform specific drug

111   screening tests. We co-cultured human and mouse CD31-/CD45-/ EpCAM$^+$ lung

112   epithelial cells with CCL206 lung fibroblasts in organoids in Matrigel and exposed

113   these *in vitro* to different concentrations (1.25%, 2.5%, 5%) of cigarette smoke extract

114   (CSE) (Fig. 2a, c). The number and size of organoids established by co-culturing

115   human lung tissue derived CD31-/CD45-/EpCAM$^+$ cells and MRC5 fibroblasts was

116   significantly decreased by CSE in a concentration dependent manner at day 14 (Fig.

117   2b). The total number of murine organoids quantified at day 14 of treatment with

118   different concentrations of CSE yielded similar results and was decreased in a CSE

119   dose dependent manner as well (Fig. 2e). To specifically analyze the impact of CSE

120   on organoids derived from alveolar epithelial progenitors, we morphologically

121   subclassified organoids into airway and alveolar type[9] organoids (Fig. 2d), which

122   revealed that alveolar organoid numbers were more susceptible to cigarette smoke

123   extract exposure than airway organoids (Fig. 2e). Immunofluorescence (IF) studies

124   confirmed that the number of acetylated-α tubulin$^+$ (ACT; ciliated cell marker, airway

125   type organoids) and pro-SPC$^+$ (type II cell marker, alveolar type organoids) organoids

126   was significantly decreased by 5% CSE (Fig. 2f). The size of both organoid types was

127   decreased at day 14 (Fig. 2g).
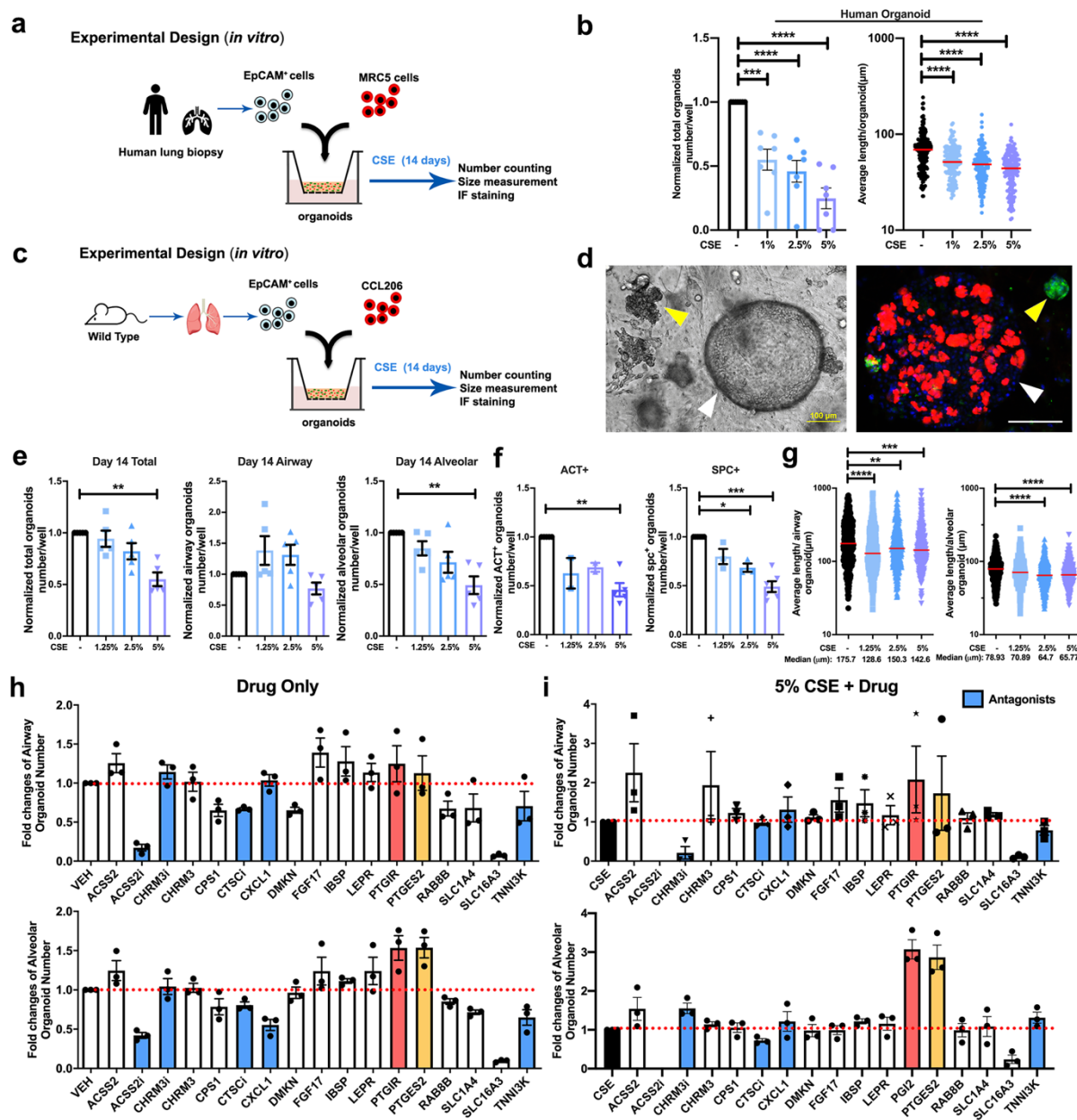
Figure 2. Cigarette smoke exposure represses adult epithelial lung organoid formation. a Schematic of *in vitro* human experimental design. **b** Quantification of total amount of human organoids and the quantification of average human organoid diameters after treatment with cigarette smoke extract (CSE) (0, 1, 2.5, and 5%). N = 7 experiments (2 healthy, 5 COPD donors). n > 150 organoids/group. **c** Schematic of *in vitro* murine experimental design. **d** Representative images of murine lung organoids. Left: light microscopy. Right: immunofluorescence of organoids. Green: pro-SPC (SPC), red: acetylated-α tubulin (ACT), blue: DAPI. White arrow: airway type of organoid, yellow arrow: alveolar type of organoid. Scale bar, 100 μm. **e** Quantification of the normalized number of total organoids, airway, and alveolar type organoids on day 14 obtained after treatment with different

138   concentrations of CSE (0, 1.25, 2.5, and 5%). **f** Quantification of normalized ACT[+] and pro-SPC[+]

139   organoids obtained after treatment with 0, 1.25, 2.5, and 5% CSE. **g** Quantification of average organoid

140   diameter after treatment with 0, 1.25, 2.5, and 5% CSE measured on day 14. N = 5 experiments, n >

141   380 organoids/group. **h-i** Overview of drug screening using the *in vitro* murine lung organoid model.

142   Comparison of the normalized number of airway and alveolar type organoids treated with the different

143   drugs of interest in the absence **(h)** or presence **(i)** of 5% CSE. Red bar: PTGIR, yellow bar: PTGES2,

144   blue: antagonists. Data are presented as mean ± SEM in number quantification. Data are presented as

145   scatter plots with medians in size quantification. For all panels: **p < 0.05, **p < 0.01, ***p < 0.001, ****p

146   < 0.0001.

147

148   We next aimed to utilize this lung organoid model to evaluate the efficacy of existing

149   COPD therapeutics. Increasing evidence[10,11] has linked phosphodiesterase (PDE) 4

150   inhibition to the therapeutic management of respiratory diseases, and roflumilast has

151   been used as an oral medication in COPD patients with a prior history of hospitalization

152   for an acute exacerbation (GOLD 2021). This led us to explore whether the classic

153   PDE4 inhibitor, rolipram, was able to rescue the CS-induced reduction in organoid

154   formation by alveolar progenitors. Thus, organoids were subjected *in vitro* to different

155   concentrations (1 and 10 μM) of rolipram in the presence and absence of 5% CSE for

156   up to 14 days (Fig.S1a). Rolipram (10 μM) alone significantly increased the total

157   number of organoids at day 7 as well as the pro-SPC[+] organoids at day 14 (Fig.S1b,

158   c), but had no beneficial effects on organoid numbers when combined with CSE

159   exposures. Treatment with rolipram (1 μM) either alone or in combination with CSE

160   induced significantly increase alveolar organoid size (Fig.S1d).

161   Budesonide is an inhaled corticosteroid used in COPD management[12–15]. Therefore,

162   we examined its effect also in our *in vitro* (Fig. S1e) and *in vivo* (Fig. S1h) CS/organoid

163   models. Intriguingly, budesonide (1-, 10-, 100 nM) in combination with CSE exposure

164   further reduced the number as well as the size of both airway and alveolar type

165   organoids as compared to CSE exposure alone (Fig. S1f, g). *In vivo* exposure to

166   budesonide together with CS increased the number of airway but not alveolar

167   organoids (Fig. S1i), without affecting organoid size (Fig. S1j). Taken together, these

168   data show that *in vitro* exposure to cigarette smoke extract functionally represses

169   human alveolar epithelial progenitor organoid formation, resulting in reduced growth

170   and differentiation, which can be mimicked using murine alveolar epithelial progenitors.

171   Validating the limitations of current pharmacology, PDE4 inhibitors and corticosteroids

172   do not prevent or reduce the detrimental effects of cigarette smoke on organoid

173   formation.

174   The assay was used subsequently to screen for the functionality of the targets in

175   restoring organoid growth. Genes downregulated in response to CS and COPD were

176   targeted with activating ligands, whereas genes upregulated in response to CS and

177   COPD were targeted using antagonists with exception of *ACSS2* and *CHRM3* for

178   which we included both an agonist and an antagonist. The effects of the drugs

179   targeting the 15 selected genes alone (compared to vehicle, Fig. 2h) and in the

180   presence of 5% CSE exposure (Fig. 2i) on the number of organoids were determined.

181   Specific information of all drug effects on organoid number and size are summarized

182   in Supplementary figure 2 and 3. Interestingly, the compound activating ACSS2

183   (Acetyl-CoA synthetase short-chain family member 2), increased the number of airway

184   type organoids and the size of alveolar organoids in combination with CSE (Fig. S2-

185   3), whereas the ACSS2 inhibitor had the opposite effects. Atropine (CHRM3

186   antagonist), IBSP (Integrin Binding Sialoprotien) and LEPR (Leptin receptor) tended

187   to increase the number and size of alveolar organoids in response to CSE as well (Fig.

188   S2-3). However, considering the overall magnitude of alveolar type organoids

189   particularly, PGE2 (target gene *PTGES*) and iloprost, (PGI2 analogue, target gene

190   *PTGIR*) were identified as the by far most promising targets with regards to their

191   capacity in restoring the CSE-induced repression of organoid formation (Fig. 2h-i, S2-

192   3).

193   **PGE2 and PGI2 significantly prevent alveolar epithelial dysfunction.** The

194   *PTGES2* and *PTGIR* genes encode membrane-associated prostaglandin E synthase

195   and the prostacyclin (PGI2) receptor, respectively. PGE2 acts on 4 receptor subtypes,

196   being *PTGER1-4*, whereas PGI2 acts primarily on *PTGIR*. We assessed their

197   expression in human lung tissue of healthy smokers and COPD patients and found

198   maintained expression of all receptors in disease with some small differences in

199   expression, most notably a reduced expression of *PTGER2* and increased expression

200   of *PTGIR* (Fig. 3a). Single cell RNAseq (sc-RNAseq) data from human lung tissue

201   shows similar expression of all 5 receptors was detected in alveolar epithelial cells and

202   in fibroblasts (http://www.copdcellatlas.com/). Single cell RNA sequencing of mouse

203   lung tissue showing that expression of *Ptger2* and *Ptger4* were highest compared to

204   that of *Ptger1* and *Ptger3* in mesenchymal cells (Fig. 3b, c). Interestingly, the

205   expression of *PTGES,* and *PTGES2*, the enzymes responsible for PGE2 synthesis

206   were relatively ubiquitous in human and mouse lung tissue, whereas *PTGIS*, the

207   enzyme responsible for PGI2 synthesis was highest in mesenchymal cell types

208   including fibroblasts. The expression of all these receptors showed lower copy

209   numbers, which is expected for G protein-coupled receptors (GPCRs).

210
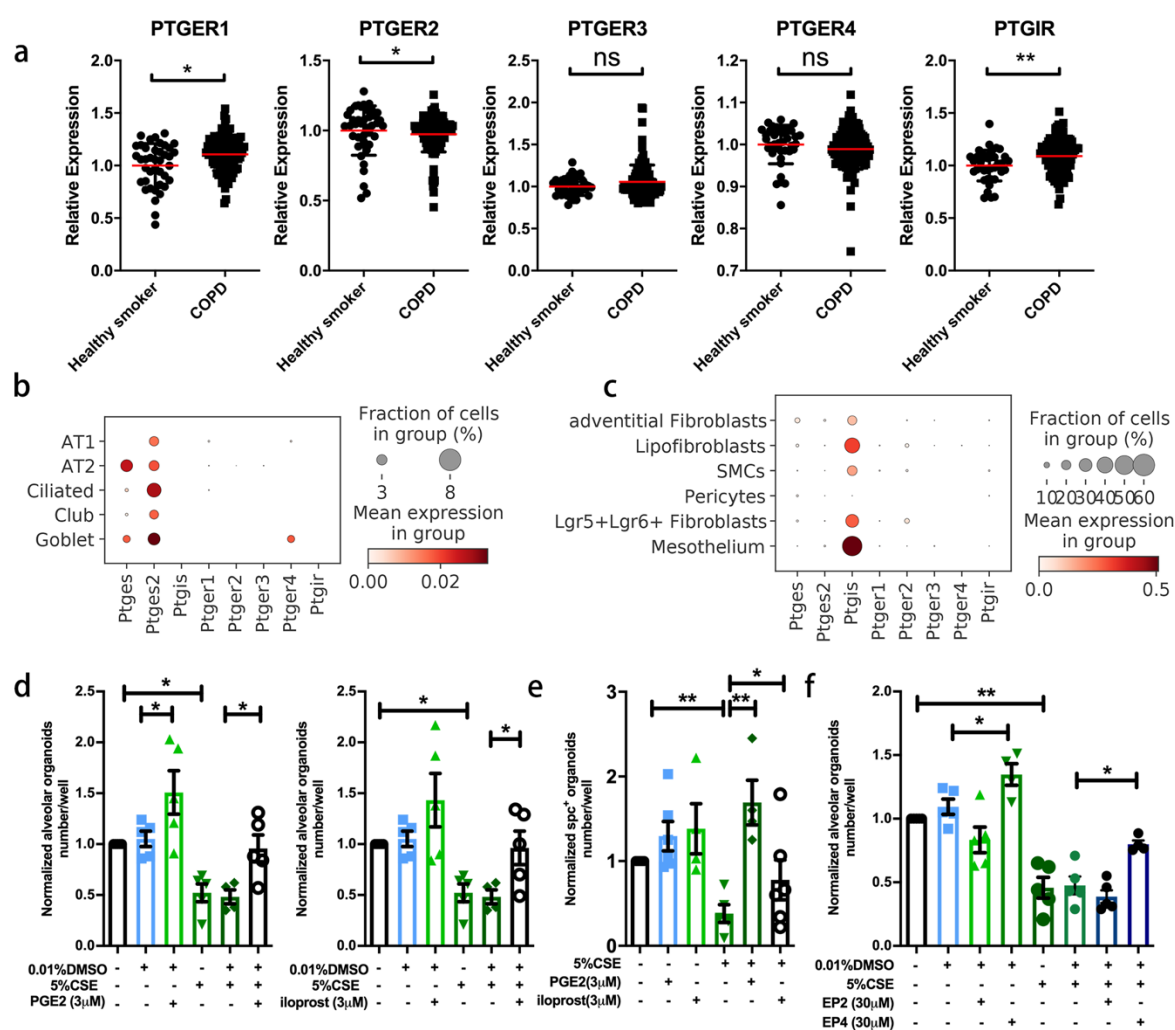
Figure 3 16,16-dimethyl prostaglandin E2, iloprost, and selective EP2 and EP4 analogues restore lung organoid formation in response to cigarette smoke (extract). a The relative gene expression of *PTGER1, PTGER2, PTGER3, PTGER4* and *PTGIR* in healthy smokers (N = 40) and COPD patients (N = 111) downloaded from the NCBI GEO database GSE76925. **b-c** Data are extracted from the NCBI GEO database GSE151674 **b** The expression *of Ptges, Ptges2, Ptgis, Ptger1, Ptger2, Ptger3, Ptger4* and *Ptgir* in epithelial cells using scRNA-seq analysis of mouse lung tissue. **c** The expression *of Ptges, Ptges2, Ptgis, Ptger1, Ptger2, Ptger3, Ptger4* and *Ptgir* in mesenchymal cells using scRNA-seq analysis of mouse lung tissue. **d** Quantification of normalized number of alveolar type organoids treated with vehicle control, or 5% CSE ± PGE2 agonist (16,16-dimethyl prostaglandin E2)/iloprost. **e** Quantification of normalized number of SPC⁺ organoids treated with vehicle control, or 5% CSE ± PGE2 agonist (16,16-dimethyl prostaglandin E2) or iloprost. **f** Quantification of normalized number of alveolar type of organoids treated with vehicle control, or 5% CSE ± selective EP2 or EP4 agonist. Data are presented as mean ± SEM. *p < 0.05, **p < 0.01, ***p < 0.001, ****p < 0.0001.

224   To further characterize the effects of PGE2 and PGI2 on defective alveolar epithelial

225   progenitors, we examined them *in vitro* (Fig. 3d-f) and *in vivo* (Fig. 4) CS(E). The PGE2

226   analogue 16,16-dimethyl prostaglandin E2 and the prostacyclin analogue iloprost both

227   increased the number of alveolar type organoids even in the presence of 5% CSE (Fig.

228   3d) and significantly increased the number of SPC$^+$ organoids under conditions of CSE

229   exposure (Fig. 3e). To address the relative roles of the two Gs-coupled PGE2

230   receptors, EP2 and EP4, we evaluated the selective agonists ((R)-Butaprost and 5-

231   [(3S)-3-hydroxy-4-phenyl-1-buten-1-yl]1-[6-(2H-tetrazol-5R-yl)hexyl]-2-pyrrolidinone,

232   CAY10598) of these receptors. Focus was on these Gs coupled receptors, as we

233   found that cholera toxin, a well-known inducer of constitutive adenylyl cyclase activity

234   and cAMP signaling, increased organoid formation both with and without the exposure

235   to CSE (Fig. S4a). The EP2 selective butaprost had no effects on organoid number

236   (Fig. 3f) but increased the alveolar size in the absence and presence of 5% CSE (Fig.

237   S5c). The EP4 selective agonist increased the number of alveolar type organoids

238   significantly and prevented the number reduction resulting from 5% CSE exposure

239   (Fig. 3f). The EP4 agonist also increased the size of both types of organoids in the

240   absence and presence of 5% CSE (Fig. S5c). To explore whether duration of drug

241   exposure affected organoid formation, the organoids were treated *in vitro* with PGE2

242   analogue or PGI2 analogue for 3 different time windows during organoid development

243   as illustrated in Supplementary figure 5d-g. These time windows were identified

244   previously[9], and mark the initial division phase (day 0-2), proliferation (day 2-7), and

245   differentiation phase (day 7-14). We observed no effects on the number of organoids

246   for any of the short-term drug treatments, suggesting continuous treatment with or

247   iloprost during all phases of organoid formation is required.

248   To examine the effects of PGE2 and PGI2 *in vivo*, we exposed mice to air (vehicle

249   control), CS, CS + misoprostol (PGE2 analogue), or CS + iloprost as shown in Figure

250   4. To assess the impact of *in vivo* cigarette smoke (CS) exposure, we isolated CD31-

251   /CD45-/EpCAM$^+$ cells from mice exposed to air or CS and co-cultured these with

252   CCL206 fibroblasts *in vitro* for 14 days (Fig. 4a). Interestingly, the number of alveolar

253   organoids was significantly decreased after *in vivo* CS exposure indicating that a

254   relatively short exposure to cigarette smoke *in vivo* is sufficient to capture early

255   changes in progenitor cell function (Fig. 4c). Cigarette smoke exposure did not change

256   the yield of CD31-/CD45-/EpCAM$^+$ cells, whereas exposing mice to misoprostol or

257   iloprost increased the yield of EpCAM+ cells (Fig. S6a). The organoid assay revealed

258   that *in vivo* (i.p.) treatment with either misoprostol or iloprost significantly increased the

259   number of alveolar type and SPC$^+$ organoids (Fig. 4e-f) *ex vivo*. Next, to investigate

260   whether *in vitro* drug treatment would have similar effects on damage caused by *in*

261   *vivo* CS exposure, we isolated EpCAM$^+$ cells from either air- or CS-exposed mice and

262   subjected these to *in vitro* misoprostol or iloprost treatment in the organoid assay for

263   14 days (Fig. 4g). *In vitro* misoprostol increased the number of alveolar type organoids

264   in cultures derived from CS-exposed mice (Fig. 4h). Only *in vitro* misoprostol increased

265   the size of alveolar organoids derived from CS-exposed animals (Fig. S6c). Taken

266   together, our data show that PGE2 and PGI2 analogues protect alveolar epithelial

267   progenitor function from the effects of CS exposure. In addition, EP4 rather than EP2

268   seems to mediate the protective effects of PGE2.
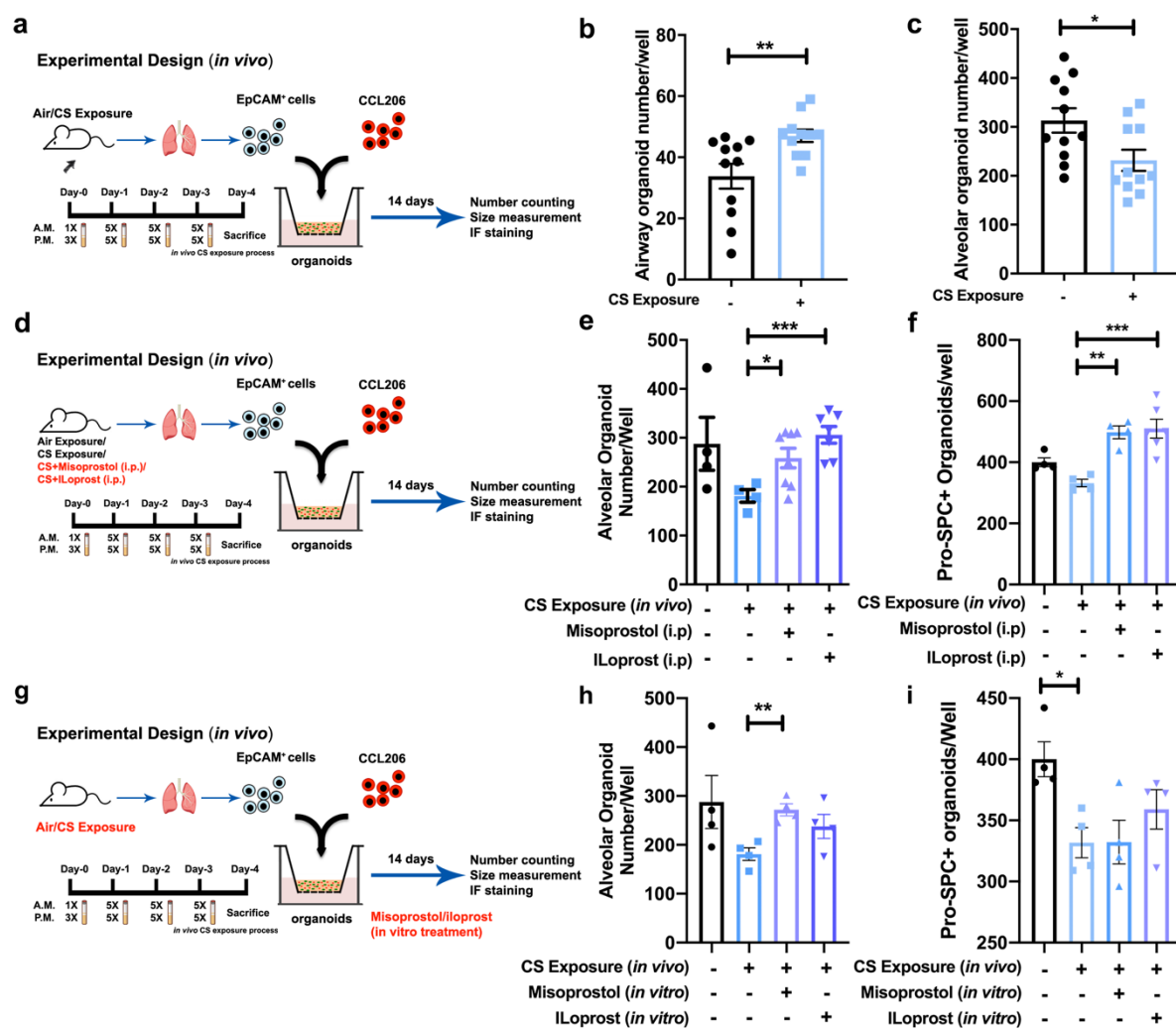
Figure 4 Administration (*in vivo* and *in vitro*) of misoprostol and iloprost to cigarette smoke-exposed mice restored lung organoid formation. a Schematic of *in vivo* CS exposure experimental setup. **b-c** Number of airway and alveolar type organoids quantified on day 14 of co-culturing CCL-206 fibroblasts and EpCAM$^+$ cells (isolated from air exposed/CS exposed mice). N = 11 experiments. **d** Schematic of experimental design. Organoids were generated from air- or CS-exposed mice treated *in vivo* with misoprostol (i.p.) or iloprost (i.p.); all organoids were treated with normal organoid medium. **e-f** Number of alveolar type and pro-SPC$^+$ organoids quantified on day 14 from co-culture of CCL-206 fibroblasts and EpCAM$^+$ cells (isolated from air- (control) and CS-exposed mice treated intraperitoneally with misoprostol or iloprost). **g** Schematic of experimental design. Organoids were generated from mice exposed to air or CS. Misoprostol and iloprost were added *in vitro* to the organoid medium for treatment. **h-i** Number of alveolar type and SPC$^+$ organoids quantified on day 14 from co-culture of CCL-206 fibroblasts and EpCAM$^+$ cells (isolated from air- and CS-exposed mice) treated with misoprostol/iloprost *in vitro*. Data are presented as mean $\pm$ SEM. *p < 0.05, **p < 0.01, ***p < 0.001, ****p < 0.0001.

283 **Distinct genetic signatures in regulation of defective alveolar epithelial repair.**

284 To unravel the transcriptional changes leading to impaired lung organoid formation

285 after exposure to CS as well as the mechanisms underlying the beneficial effects of

286 PGE2 and PGI2 treatment, we performed RNA sequencing (Fig. 5a) on EpCAM$^+$ cells

287 isolated from mice exposed to air (control), CS, CS + misoprostol(i.p.), or CS + iloprost

288 (i.p.), directly after the isolation procedure (i.e., prior to inclusion in the organoid assay).

289 Principal-component analysis (PCA) revealed that the CS-exposed group is

290 transcriptionally distinct from the control group (Fig. 5b), and that the CS/misoprostol

291 and CS/iloprost groups are transcriptionally different from the CS exposed group. The

292 top 20 differentially expressed genes from these three comparisons, including both

293 up- and downregulated genes, are shown in the heatmaps (Fig. 5c) and summarized

294 in supplementary materials. Reactome pathway analysis was used to identify

295 molecular pathways overrepresented in CS/misoprostol/iloprost-modulated genes in

296 alveolar epithelial cells. Within the top 20 enriched pathways (Fig. 5d, supplementary

297 materials), genes associated with cell cycle, mitotic prometaphase, DNA

298 replication/synthesis and RHO GTPases activate formins signaling pathways were

299 upregulated by CS exposure compared to air (control) exposure, however, these were

300 downregulated by treatment with misoprostol or iloprost. Notably, genes associated

301 with the circadian clock signaling pathway were downregulated by CS exposure but

302 restored by treatment with misoprostol or iloprost. Moreover, signaling by FGFR1, 3

303 and 4 were downregulated in response to CS exposure, whereas the same signaling

304 pathways were upregulated by misoprostol but not iloprost treatment. These findings

305 suggest that the repairing mechanisms of misoprostol and iloprost in response to CS

306 were common in cell cycle and circadian clock signaling and the distorted FGFR

307 signaling resulted from CS was corrected by misoprostol uniquely. In addition, the

308   nuclear receptor transcription pathway, growth hormone receptor signaling, MAPK,

309   WNT and cell-cell communication signaling pathways appear to downregulate in

310   response to CS, which were not observed in either misoprostol/iloprost treatment

311   group. Overall, the RNA-seq analysis demonstrates both common and distinct

312   transcriptomic mechanisms of misoprostol and iloprost treatment in response to CS

313   exposure in alveolar epithelial progenitors.

314
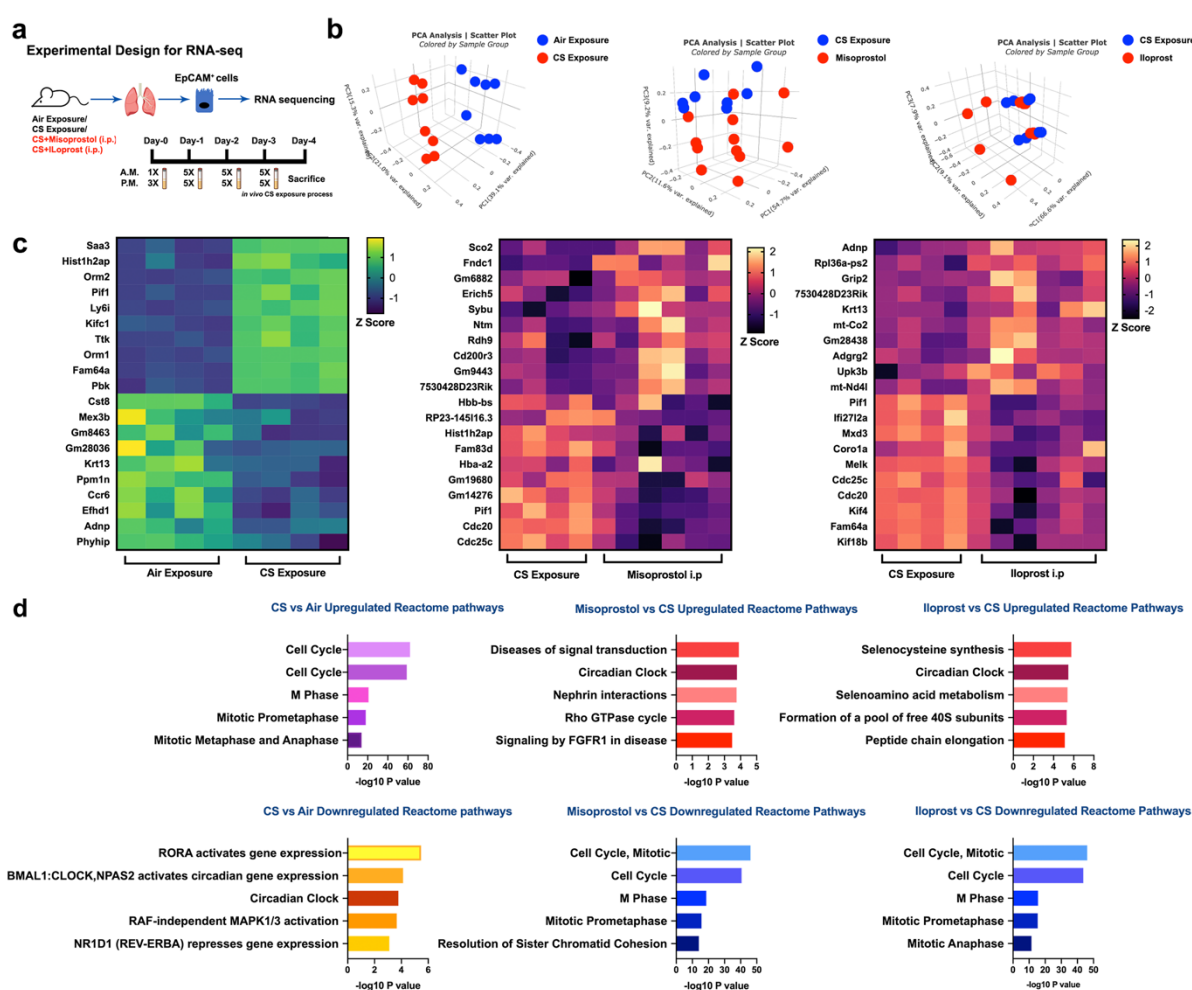
Figure 5 Transcriptomic signatures in response to cigarette smoke with(out) misoprostol and iloprost. a Schematic experimental design for RNA sequencing. **b** PCA plots demonstrate the clusters betweern different comparisons: air vs CS, CS vs CS+misoprostol, and CS vs CS+iloprost. **c** Heatmaps displaying the top 20 differentially expressed genes in air vs CS, CS vs CS+misoprostol, and CS+iloprost exposed epithelial cells. **d** The top 5 significantly up- and downregulated reactome

320   pathways enrichment form differentially expressed genes within the comparisons of air vs CS exposure,

321   CS exposure vs CS+misoprostol, and CS exposure vs CS+iloprost.

322

323   **Discussion**

324   Chronic obstructive pulmonary disease results from repeated micro-injuries to the

325   epithelium often caused by tobacco smoking. In susceptible individuals, this results in

326   tissue remodeling in the conducting airways and destruction of the respiratory

327   bronchioles and alveoli[19]. No clinically approved pharmacological treatment prevents

328   or reverses the tissue destruction in the distal lung. The results of our study are in line

329   with this contention and demonstrate that the PDE4 inhibitor rolipram and the

330   corticosteroid budesonide had no, or only very limited, beneficial effects on impaired

331   organoid growth and differentiation in response to cigarette smoke extract *in vitro* or

332   in response to cigarette smoke exposure *in vivo*. In fact, if anything, budesonide

333   appeared to restrict progenitor cell growth, which is a concern given the wide use of

334   corticosteroids in the management of COPD. This underscores the need for novel drug

335   targets.

336   Consequently, we set out to search for new potential drug targets for lung repair in

337   COPD and identify EP and IP receptor agonists as two such potential targets, by

338   utilizing a transcriptomics-guided drug discovery strategy. Both EP and IP receptor

339   agonists were able to promote epithelial repair responses after exposure to cigarette

340   smoke (extract). Whereas PGE2 and PGI2 showed the most profound changes, other

341   methods including ACSS2 agonism, LEPR agonism and IBSP agonism yielded

342   smaller effects. ACSS2 supports acetyl-CoA synthesis from acetate in the cytosol[20,21],

343   and thereby plays an important role in lipid metabolism and in the regulation of histone

344   acetylation in the nucleus during gene transcription. IBSP is a member of the small

345   integrin-binding ligand N-liked glycoprotein (SIBLING) family[22,23], which is associated

346   with bone metastases of lung cancer[24]. LEPR (leptin receptor), is an adipocytokine

347   that has a central role in regulating food intake and energy expenditure[25], but has also

348   been linked to lung function decline in a population in COPD[26]. Nonetheless, among

349   all the candidate targets, PGE2 (*PTGES2*) and PGI2 (*PTGIR*) analogues emerged as

350   the most promising compounds among all drugs in the current study. Prostaglandins

351   (PGs) are lipid mediators synthesized from arachidonic acid (AA) via the

352   cyclooxygenase pathway, and include PGD2, PGI2, PGH2, PGE2 and PGF2α[27]. PGI2

353   signals via IP receptors to induce cAMP signaling, similar to EP4 receptors. We show

354   EP4 receptors to have similar expression as in non-COPD controls, whereas IP

355   receptors are expressed at higher levels in COPD patients indicating the expression

356   of both receptors is maintained in disease.

357   We show that PGE2 agonists are beneficial in reducing CS-induced damage in

358   alveolar epithelial progenitors. However, PGE2 has been reported as an unstable

359   molecule with an extremely short half-life; therefore, targeting its receptors with

360   specific more stable analogues may be a better alternative. PGE2 is the most widely

361   produced PG in the human body and it signals via four specific G-protein-coupled

362   receptors (EP1-4[28,29]). The interactions between PGE2 and EP receptors depend on

363   tissue and cell type, specific receptor expression, and differences in binding affinities,

364   leading to unique patterns of EP receptor activation[30]. PGE2 can stimulate cAMP

365   production through EP2 and EP4 receptors, whereas EP3 activation results in

366   decreased cAMP synthesis and EP1 stimulation is coupled to Gq-activation and

367   (enhanced) Ca^{2+} signaling[27,30,31]. EP1 and EP3 receptors can mediate

368   bronchoconstriction indirectly through activation of neural pathways[32], as a

369   consequence non-selective PGE2 analogues are unsuitable as pulmonary drugs.

370 Therefore, we selected analogues of EP2 and EP4 to mimic effect of PGE2 in our

371 organoid assay, and demonstrated that EP4 agonism showed beneficial effects

372 against impaired organoid formation in response to (CS)E exposure. Targeting EP4

373 receptors is worthwhile investigating in more detail in the future, as the effects may

374 surpass epithelial repair only. Additional beneficial effects of EP4 agonism in COPD

375 may include bronchoprotection[33] and inhibition of inflammation[34], suggesting that EP4

376 agonism could unify several functional features that support the treatment of COPD,

377 making this an intriguing pharmacological target.

378 Iloprost, a stable PGI2 analogue [27,35–39], has been shown to have anti-inflammatory

379 effects and protects against bleomycin-induced pulmonary fibrosis in mice[36], and is

380 also clinically used for the treatment of pulmonary hypertension[35]. Although a recent

381 study[38] showed iloprost improved clinical outcomes in COPD patients with poor lung

382 oxygenation, its impact on alveolar repair is unknown. Here we show that iloprost

383 prevents the repressed organoid formation resulting from CS(E) exposure.

384 By generating transcriptomic signatures of epithelial progenitors derived from mice

385 exposed *in vivo* to air, CS, CS + misoprostol or CS + iloprost, we uncovered dynamic

386 molecular signaling pathways in response to CS exposure. Intriguingly, we identified

387 circadian clock signaling as being significantly repressed in the alveolar epithelial

388 progenitors derived from mice exposed to CS, which could be improved by either

389 misoprostol or iloprost treatment. Circadian rhythms[40–43] are normally generated and

390 regulated by clock genes, including *BMAL1* (*ARNTL1*) and *CLOCK* encoding

391 activators, period (*PER1-3*) and cryptochrome genes (*CRY1-2*) that encode

392 repressors, and the nuclear receptors Rev-erb (*NR1D1* and *NR1D2*) and *RORA* which

393 constitute secondary regulatory loops. These core clock genes not only activate or

394 repress a cell-autonomous clock, but also regulate the clock-controlled genes

395   (CCGs)[44], thus interacting with other molecular signaling pathways. Previously, it has

396   been demonstrated that clock signaling is downregulated in CS exposed mice, linked

397   to an impairment of anti-oxidant defense mechanisms[45] and Rev-erbα has been

398   shown as an key regulator of inflammatory response in lung injury models[16–18,46]

399   Furthermore, we found that CS exposure upregulated pathways associated with cell

400   cycle activity in alveolar epithelial progenitors, which could be counteracted by *in vivo*

401   misoprostol or iloprost treatment. The cell cycle[47–51] is driven by a set of tightly

402   regulated molecular events controlling DNA replication and mitosis with four phases,

403   and each individual cell may require different triggers in order to decide whether to

404   enter proliferation or apoptosis. To further assess alveolar epithelial progenitors under

405   which cell cycle/apoptotic status in response to CS exposure as well as additional

406   PGE2/PGI2 treatments may be the next step to investigate in the future. A link between

407   circadian clock and cell cycle signaling pathways has been proposed[44,50,52].

408   Importantly, the molecular control of the biological clock is dependent on cAMP

409   signaling and cAMP activators are known to entrain the biological clock[53], explaining

410   the link between PGE2 and PGI2 activation and restoration of the defective clock

411   signaling in combination with CS exposure. Hence, it is of great interest to determine

412   in more molecular detail how these two oscillatory systems communicate in regulating

413   PGE2/PGI2-mediated lung repair in future studies.

414   In conclusion, in this study we demonstrate for the first time the protective effects of

415   several drug candidates, and in particular PGE2 and PGI2 analogues, against *in vivo*

416   and *in vitro* CS(E)-induced damage of alveolar epithelial progenitors. Furthermore,

417   using transcriptome analysis, we show that CS induces a wide range of transcriptional

418   changes, including alterations of circadian clock and cell cycle signaling pathways,

419   which can be counteracted by either misoprostol (PGE2) or iloprost (PGI2) treatment.

420   Overall, these data provide promising therapeutic strategies to specifically address

421   defective lung repair in respiratory diseases, in particular targeting EP4 and IP

422   receptors.

Methods

Animals. All mouse experiments for organoid study were performed at the Central Animal Facility (CDP) of the University Medical Center Groningen (UMCG) in accordance with the national guidelines and upon approval of the experimental procedures by CDP and the Institutional Animal Care and Use Committee (IACUC) of the University of Groningen (CCD license AVD105002015303). C57BL/6J (555) and BALB/cByJ (Jax-strain) mice (both genders, 8–12 weeks of age) were maintained under 12-h light/ dark cycles and were allowed food and water ad libitum. Animals for circadian clock studies were exposed to CS and/or administrated with compounds at the same time of the day for all mice in all groups. Animals were euthanized at the same time of the day. Adult (female, 8-10 weeks of age) C57BL/6N mice were obtained from Charles River (Sulzfeld, Germany) for the single cell RNAseq analysis of lungs following exposure to chronic CS. These experiments were performed at the Helmholtz Zentrum München and approved by the ethics committee for animal welfare of the local government for the administrative region of Upper Bavaria (Regierungspräsidium Oberbayern) and were conducted under strict governmental and international guidelines in accordance with EU Directive 2010/63/EU.

Human material. The human lung tissue was obtained from lung transplant donors according to the Eurotransplant guidelines including the absence of primary lung diseases such as asthma and COPD, and no more than 20 pack years of smoking history[54]. Gene expression in human lung published data sets was obtained by down loading series matrix files from the NCBI GEO database for GSE76925[55] and gene expression normalized to healthy smokers.

448   ***In vivo* cigarette smoke exposure.** Mice (n = 4–11/group, 10-12 weeks old) were

449   exposed (whole body) to 3R4F research cigarettes (Tobacco Research Institute,

450   University of Kentucky, Lexington, KY) for four consecutive days (two sessions/day, 8

451   hours between each exposure) to establish an acute smoke-induced inflammation

452   model, as described previously[8]. In the cigarette smoke (CS) group, mice were

453   exposed to 1 cigarette in the morning and 3 in the afternoon on day 1. From day 2 to

454   4, mice were exposed to 5 cigarettes each session. All cigarettes were smoked without

455   a filter in 5 min at a rate of 5L/h in a ratio with 60 L/h air using a peristaltic pump (45

456   rpm, Watson Marlow 323 E/D, Rotterdam, NL). In the control group, mice were

457   exposed to fresh air using similar exposure chambers as the CS group.

458   In some studies, budesonide was nebulized (0.1 mM, 15 min/mouse/exposure) to

459   wild-type mice (n = 6) prior to each CS exposure. In separate studies, intraperitoneal

460   (IP) injections of 50 μg misoprostol or 50 μg iloprost were given 30 min to wild-type

461   mice (n = 6-8) prior to each CS exposure. On day 5, mice were sacrificed, and the

462   lungs were immediately used for establishing organoid cultures or stored at - 80°C for

463   further experimental uses.

464   For the single cell RNAseq analysis of lungs CS was generated from 3R4F

465   Research Cigarettes with the filters removed. Mice were whole body exposed to active

466   100% mainstream CS of 500 mg/m^3 total particulate matter (TPM) for 50 min twice per

467   day for 4m in a manner mimicking natural human smoking habits as previously

468   described[55]

469

470   **Fibroblast culture.** Mouse fibroblasts, CCL206 (Mlg [CCL206], ATCC, Wesel,

471   Germany) were cultured in DMEM/F12 medium supplemented with 10% (v/v) fetal

472   bovine serum, 100 U/mL penicillin/streptomycin, 2 mM L-glutamine, and 1%

473   amphotericin B in a humidified atmosphere under 5% CO_2/95% air at 37°C, as

474   previously described[6,9,56]. For organoid experiments, fibroblasts were proliferation-

475   inactivated by incubation in mitomycin C (10 µg/mL, Sigma, M4287) for 2 h, followed

476   by 3 washes with PBS after which the cells were trypsinized before introduction into

477   the organoid co-cultures. Human lung fibroblasts MRC5 (CCL-171; ATCC, Wesel,

478   Germany) were cultured in Ham's F12 medium supplemented with the same additives

479   as the murine fibroblasts medium.

480

481   **Cigarette smoke extract (CSE).** The smoke of two 3R4F research cigarettes was

482   pumped into 25 mL warm fibroblasts culture medium to produce 100% cigarette smoke

483   extract (CSE)[11]. All cigarettes were without a filter and smoke was passed through the

484   medium using a peristaltic pump (45 rpm, Watson Marlow 323 E/D, Rotterdam, NL).

485   CSE was freshly prepared before each set of experiments.

486

487   **Organoid culture.** The organoid culture system is based on previously published

488   protocols from our group[6,9,56]. In brief, epithelial cells (CD31$^-$/CD45$^-$/CD326$^+$) were

489   freshly isolated from murine or human lung tissue and co-cultured with murine CCL206

490   or human MRC5 fibroblasts, respectively, in Matrigel® (Corning Life Sciences B.V.,

491   Amsterdam, The Netherlands). EpCAM$^+$ (CD31$^-$/CD45$^-$/CD326$^+$) cells were isolated

492   from mouse lung tissue (without the trachea) using the QuadroMACS™ Separator and

493   antibody-bound magnetic beads (Miltenyi Biotec, Leiden, The Netherlands). EpCAM$^+$

494   cells and fibroblasts were mixed 1:1 (20,000 cells each) and suspended in 100 µL of

495   Matrigel prediluted 1:1 (v/v) with DMEM supplemented with 10% FBS. This mixture of

496   cells was added to a 24-well Falcon® cell culture insert (Corning, USA) within a 24-

497   well plate containing 400 µL of organoid media (DMEM/F-12 supplemented with 5%

498   FBS, 1% penicillin/streptomycin, 1% glutamine, 1% amphotericin B, 0.025‰ EGF, 1%

499   insulin-transferrin-selenium, and 1.75‰ bovine pituitary extract) underneath the insert

500   in each well. Adult human donor tissue was isolated from histologically normal regions

501   of lung tissue specimens obtained at University Medical Centre Groningen (Groningen,

502   The Netherlands) from n = 7 patients (2 non-COPD and 5 COPD patients). Human

503   lung tissues were incubated and homogenized overnight in an enzyme mixture at 4 °C;

504   the EpCAM⁺ isolation process was similar to that described above for murine lung

505   tissue. Organoids were cultured in a humidified atmosphere under 5% CO_2/95% air at

506   37 °C and medium in the wells was refreshed every 2–3 days. To quantify the number

507   of organoids, light microscopy at 20x magnification was used and organoids were

508   counted manually. The diameter of the organoids (organoid size) was measured using

509   NIS-Elements software with a light microscope.

510   For *in vitro* organoid experiments, organoids were continuously treated with control,

511   1.25% (1% for human organoids), 2.5% or 5% CSE and organoid culture medium was

512   refreshed every other day. All information on the pharmacological compounds used in

513   this study is provided in the Supplementary table 1.

514

515   **Immunofluorescence staining.** The immunofluorescence staining assay for

516   organoids was performed as described previously by our group with minor

517   modifications[6,9,56]. Organoids were fixed in acetone diluted 1:1 (v/v) with methanol for

518   15 min at –20 °C. After fixation, one mL of PBS with 0.02 % sodium azide was added

519   to the well underneath the insert. Organoids were kept at 4°C for one week after

520   fixation. BSA media was added on top of the insert for blocking at room temperature

521   (RT) for 2h. Afterwards, primary antibody incubation was performed in PBS buffer with

522   0.1% BSA and 0.1% Triton X-100 overnight at 4 °C. The next day, the organoids were

523 washed with PBS for 30 min three times and secondary antibody incubation was

524 performed for 2h at RT. After washing with PBS for 15 min, the organoids on the insert

525 membrane were transferred to a glass slide with two drops of mounting medium

526 containing DAPI (Abcam 104139, Cambridge, UK), and a coverslip was applied.

527   The slides were kept at 4 °C. Confocal images were acquired using a Leica SP8

528 microscope or a Leica DM4000B microscope. Images were obtained and analyzed

529 with LASX (Leica) software (open resource, Leica Microsystems GmbH, Wetzlar,

530 Germany).

531

532 **RNA extraction and RNA sequencing (RNA-seq) analysis.** The EpCAM$^+$ cells

533 isolated from mice exposed to Air, CS, CS+misoprostol, or CS+iloprost were used to

534 extract total RNA for RNA sequencing using NucleoSpin® RNA kit (Machery-Nagel,

535 740955, Germany) according to the manufacturer's instructions. RNA concentrations

536 and qualities were analyzed using Nanodrop spectrophotometer. An Illumina NovaSeq

537 6000 sequencer was used for RNA-seq data analysis by GenomeScan

538 (https://www.genomescan.nl). The procedure included data quality control, adapter

539 trimming, alignment of short reads and feature counting. Library preparation was

540 checked by calculating ribosomal (and globin) content. Checks for possible sample

541 and barcode contamination were performed and a set of standard quality metrics for

542 the raw data set was determined using quality control tools (FstQC v0.34 and FastQA).

543 Prior to alignment, the reads were trimmed for adapter sequences using Trimmomatic

544 v0.30. To align the reads of each sample, the ensemble mouse reference GRCm38

545 (patch 6) was used. Data analyses following the RNA-seq studies were performed

546 using the BioJupies platform (https://amp.pharm.mssm.edu/biojupies/)[57]. Gene

547   expression in murine lung published data sets was obtained by downloading series

548   matrix files from the NCBI GEO database GSE151674.

549

550   **Statistics analysis.** All data are presented as mean $\pm$ SEM unless indicated otherwise.

551   Unless stated otherwise, all data were assessed for statistical significance using two-

552   tailed Student's t-test or one-way ANOVA. The p-value indicating statistically

553   significant differences between the mean/median values are defined as follows: *p <

554   0.05, **p < 0.01, ***p < 0.001, ****p < 0.0001. Statistical analyses were performed with

555   GraphPad Prism 8 software.

Author Contributions:

Author X.W., R.G. conceptualized the project, analyzed and interpreted the data; R.G., L.E.M.K., and M.S. supervised the project; X.W., A.M., M.K., L.E.M.K., A.Ö.Y., and R.G. assisted designing the experiments; X.W., S.B., V.V., L.A.V., and A.D'M. performed the experiments; X.W., T.M.C., and M.A. prepared the figures; T.M.C., M.A., H.B.S., and A.Ö.Y. assisted in bioinformatics analysis; X.W., and R.G. wrote the manuscript; All authors reviewed and commented on the manuscript and agreed to the final version.

Competing interest:

Author V.V. and L.E.M.K. are employees of Aquilo BV. Author R.G. and M.K. are members of the BREATH consortium funded by the Lung foundation Netherlands (Longfonds). All other authors declare no competing interests.

Supplementary tables and figures

Supplementary Table 1 Information of final drug lists screened on organoid assay.

NO	Overlap Up	Full name	Drug/compound name	Final concentrations	Article No.	Company
1	CPS1	Carbamoyl-phosphate synthase 1	**N-Acetyl-L-glutamic acid**	10 µM	855642-25G	Sigma-Aldrich
2	CTSC	Cathepsin C/Dipeptidyl peptidase 1	Cathepsin c inhibitor	1 µM	BI-9740	Boehringer Ingelheim
3	CXCL1	C-X-C Motif Chemokine Ligand 1	Reparixin (L-Lysine salt)	100 nM	Cayman - 21492	Cayman chemical
4	DMKN	Derrmokine	Dermokine beta recombinant protein antigen	100 ng/mL	NBP1-86840PEP	Novus Biologicals
5	PTGIR	Prostaglandin I2 Receptor	iloprost	0.03-, 0.3-, 3 µM	SML1651	Sigma-Aldrich
6	RAB8B	RAB8B, Member RAS Oncogene Family	CHEMBL384759/Guranosine 5'-diphosphate sodium salt (GDP)	10 µM	G7127	Sigma-Aldrich
7	TNNI3K	TNNI3 Interacting Kinase	GSK-114	10 µM		

NO	Overlap Down	Full name	Drug/compound name		Article No.	Company
1	ACSS2	Acyl-CoA Synthetase Short Chain Family Member	Acetyl coenzyme A sodium salt	10 mM	A2056-1MG	Sigma-Aldrich
2	ACSS2i	2	ACSS2 inhibitor	10 mM	S8588	Selleckchem.com
3	CHRM3	Cholinergic Receptor Muscarinic 3	Methacoline	10 µM	A2251	Sigma-Aldrich
4	CHRM3i		Atrophine	1 µM	A0132	Sigma-Aldrich
5	FGF17	Fibroblast Growth Factor 17	Recombinant human FGF-17 protein	10 ng/mL	319-FG-025	R&D systems
6	IBSP	Integrin Binding Sialoprotein	Recombinant Human IBSP/Sialoprotein II Protein, CF	10 ng/mL	4014-SP-050	R&D systems
7	LEPR	Leptin Receptor	Recombinant Mouse Leptin Protein, CF	100 ng/mL	L4146-1MG	Sigma-Aldrich
8	PTGES2	Prostaglandin E Synthase 2	16,16-dimethyl Prostaglandin E2	0.03-, 0.3-, 3 µM	D0160	Sigma-Aldrich
			Misoprostol	3 µM	M6807	Sigma-Aldrich
9	SLC16A3	Solute Carrier Family 16 Member 3	Streptozocin	10 µM	S0130-50MG	Sigma-Aldrich
10	SLC1A4	Solute Carrier Family 1 Member 4	L-Alanine	100 µM	A7627-1G	Sigma-Aldrich

577

Supplementary Table 2 Information of compounds used in organoid assay.

Name	Final concentrations	Article No.	Company
Rolipram	1-, 10 µM	R6520	Sigma-Aldrich
Budesonide	1-, 10-, 100 nM	B7777	Sigma-Aldrich
Cholera toxin	0.1 mg/mL	C8052	Sigma-Aldrich
(R) -Butaprost (EP2 analogue)	30 µM	B6309	Sigma-Aldrich
EP4 analogue*	30 µM	CAY10598	Cayman chemical
Forskolin	10 µM	F6886	Sigma-Aldrich
IBMX (3-Isobutyl-1-methylxanthine)	100 µM	Obtained from AppliChem (Germany)	
db-cAMP (Bucladesine)	100 µM	D0627	Sigma-Aldrich
Olodaterol	100 nM	Obtained from AppliChem (Germany)	

578   *EP4 analouge: 5-[(3S)-3-hydroxy-4-phenyl-1-buten-1-yl]1-[6-(2H-tetrazol-5R-yl)hexyl]-2-pyrrolidinone
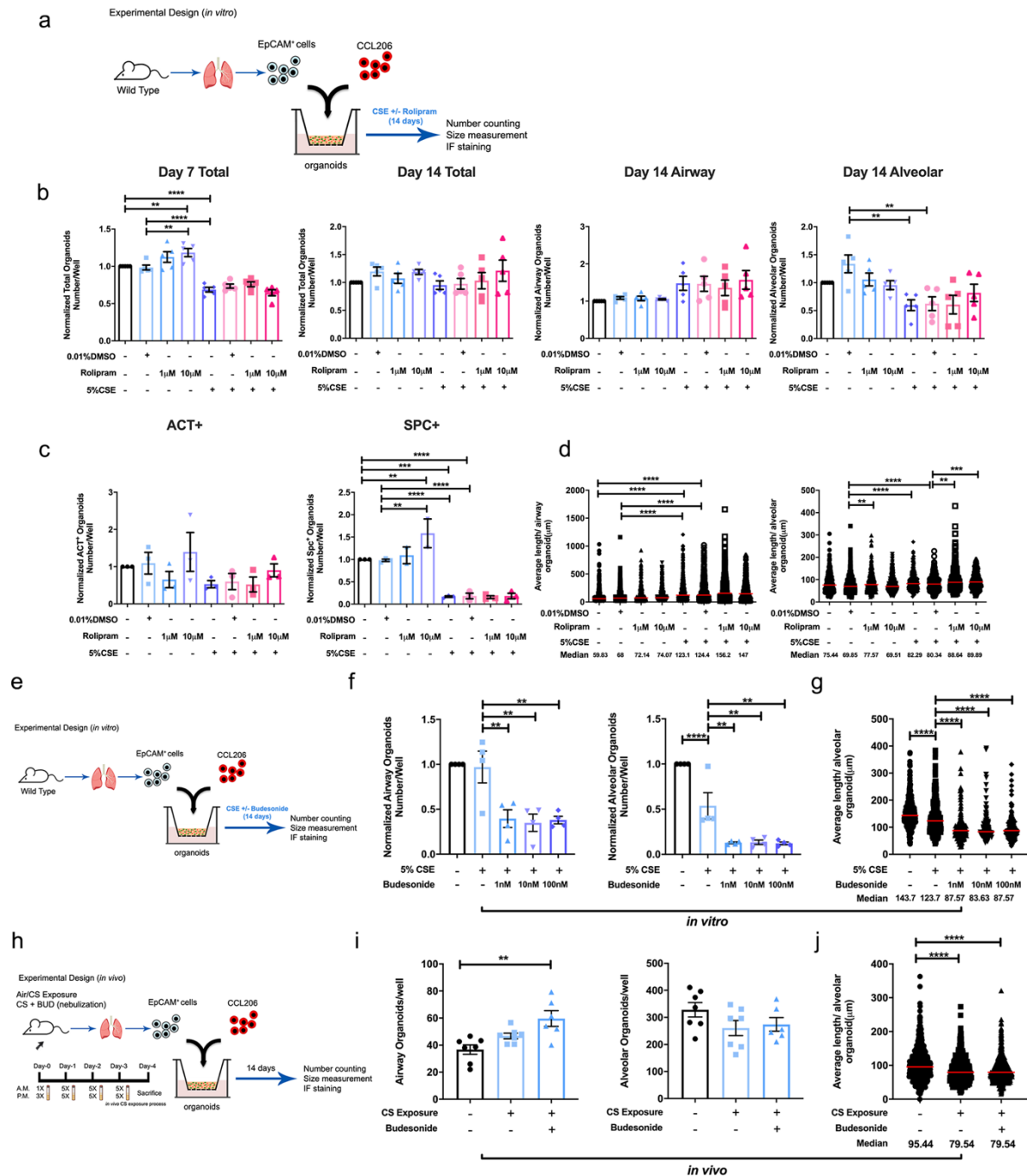
579

580 **Supplementary figure 1. Effect of Rolipram and Budesonide on lung organoid formation.**

581 **a** Schematic of *in vitro* experimental design. **b** Quantification of normalized number of total organoids

582 (day 7), total organoids (day 14), airway type organoids (day 14), alveolar type organoids (day 14)

583 treated with 5% CSE $\pm$ rolipram (0-, 1-, 10μM). **c** Quantification of normalized ACT$^+$ and SPC$^+$ organoid

584 numbers treated with 5% CSE $\pm$ rolipram (0-, 1-, 10μM) at Day 14. **d** Quantification of average length

585 (diameter) of airway and alveolar type organoids treated with 5% CSE $\pm$ rolipram (0-, 1-, 10μM)

586 measured on day 14. N = 5 experiments, n > 503 organoids/group. Data are presented as scatter plots

587   with medians. **e** Schematic of *in vitro* experimental design. **f** Quantification of normalized number of

588   airway and alveolar type organoids treated with 5% CSE $\pm$ Budesonide (0-, 1-, 10-, 100 nM) measured

589   on day 14. **g** Quantification of average length (diameter) of alveolar type organoids (median value)

590   treated with 5% CSE $\pm$ Budesonide (0-, 1-, 10-, 100 nM) measured on day 14. N = 4 experiments, n >

591   165 organoids/group. Data are presented as scatter plots with medians. **h** Schematic of *in vivo*

592   experimental design. **i** Number of airway and alveolar type organoids from co-culture of CCL-206

593   fibroblasts and EpCAM^{+} cells (isolated from air-exposed, CS-exposed, and CS-exposed + Budesonide

594   nebulized mice) quantified on day 14. **j** Quantification of average length (diameter) of alveolar organoids

595   (median value) from co-culture of CCL-206 fibroblasts and EpCAM^{+} cells (isolated from air-exposed,

596   CS-exposed, and CS-exposed + Budesonide nebulized mice) on day 14. N = 6 - 7 experiments, n >

597   671 organoids/group. Data are presented as scatter plots with medians. **p < 0.05, **p < 0.01, ***p <
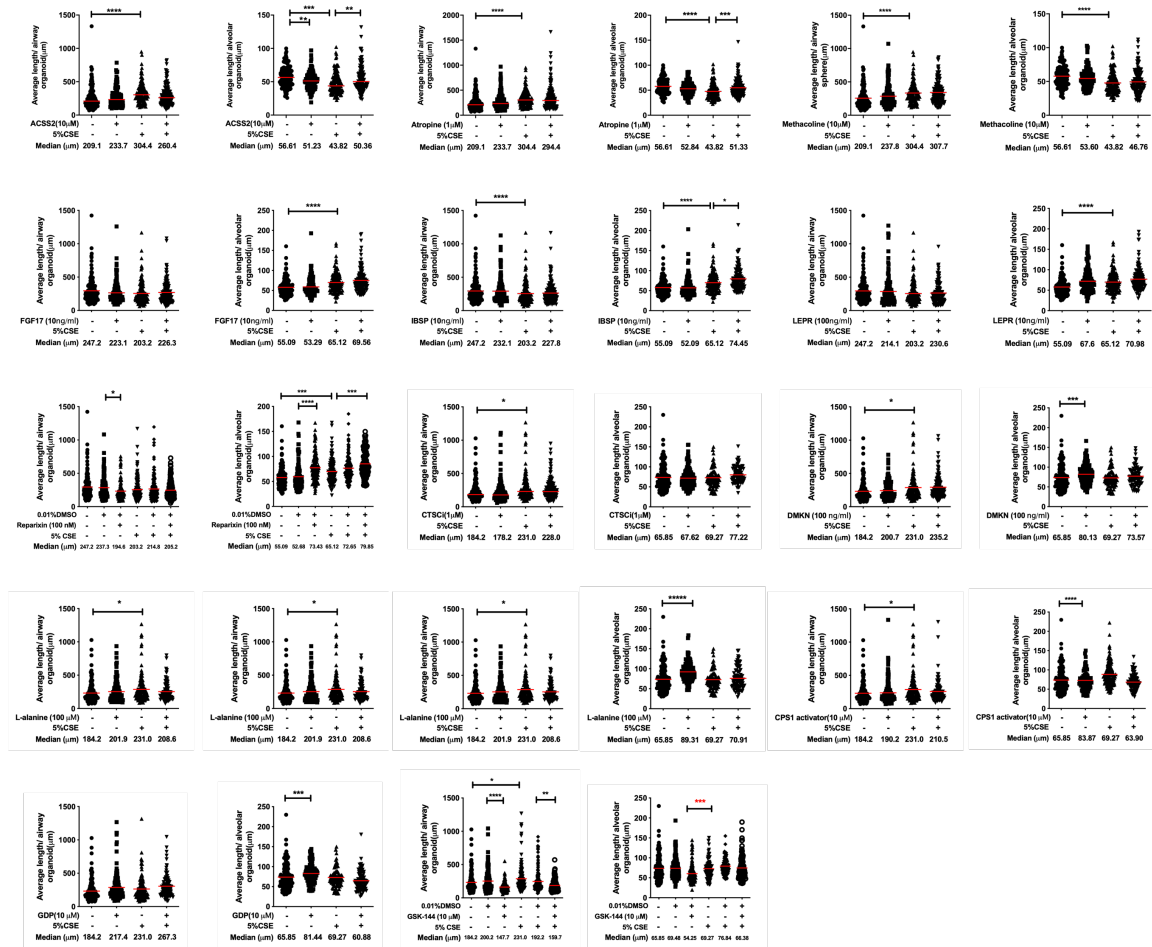
598   0.001, ****p < 0.0001

599
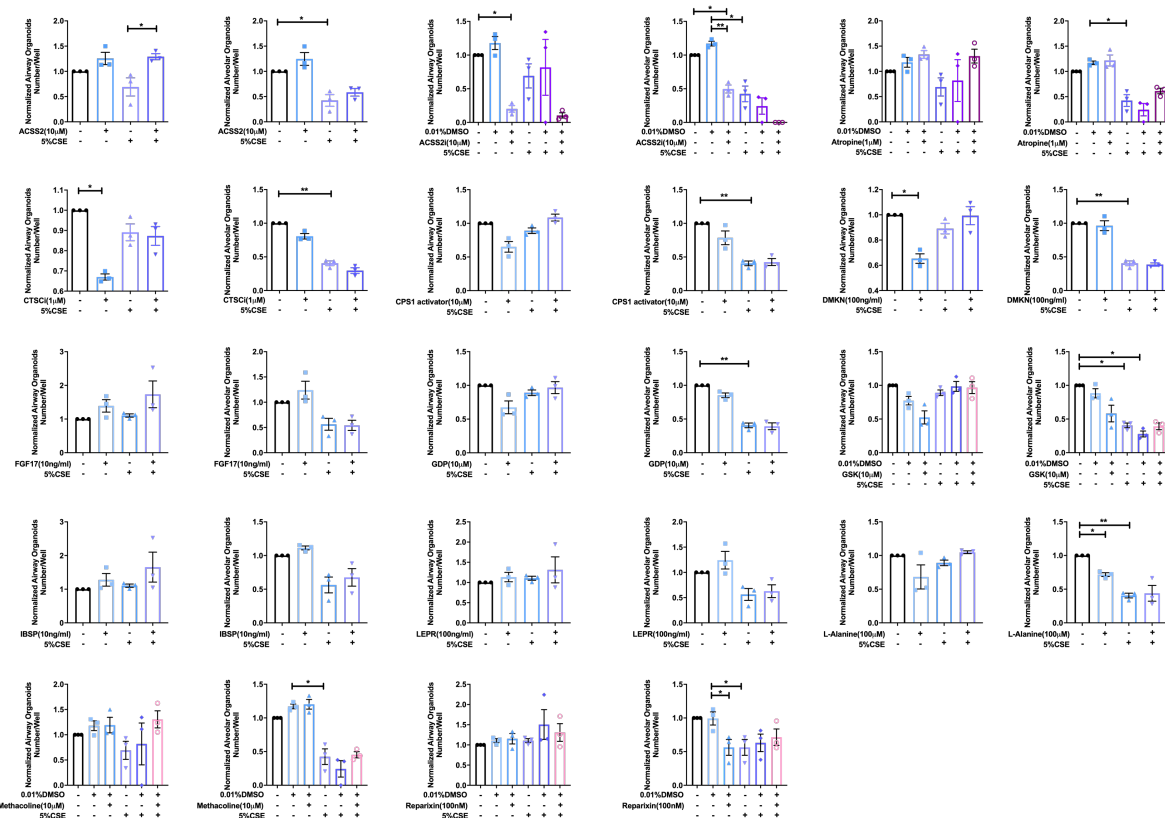
Supplementary figure 2 Effects of 15 drugs candidates of interest (including an additional agonist and antagonist for one gene target) on the normalized number of airway and alveolar type lung organoids in the presence and absence of 5% CSE. Data are presented as median $\pm$ SEM. **$p < 0.05$, **$p < 0.01$, ***$p < 0.001$, ****$p < 0.0001$.

Supplementary figure 3 Effects of 15 drugs candidates of interest (including an additional agonist and antagonist for one gene target) on the size of airway and alveolar type lung organoids in the presence and absence of 5% CSE. Data are presented as median $\pm$ SEM. **$p < 0.05$, **$p < 0.01$, ***$p < 0.001$, ****$p < 0.0001$.
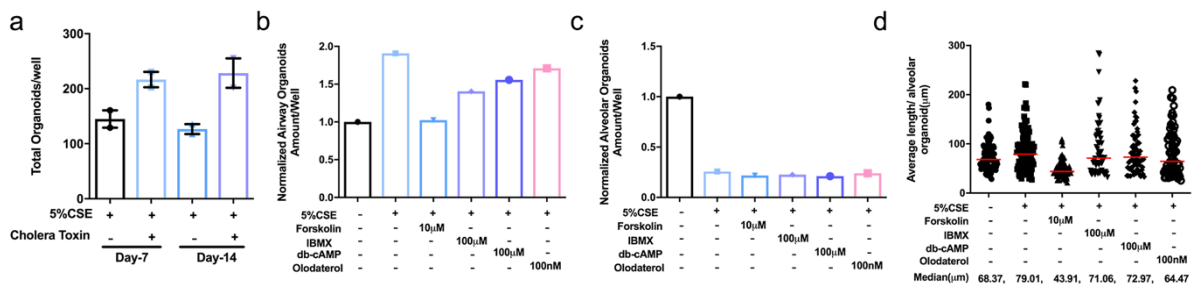

Supplementary figure 4 Compounds related to cAMP signaling pathways tested on lung organoid assay. a Quantification of total organoids treated with 5% CSE + cholera toxin at different time points. **b** Quantification of normalized airway type organoids treated with 5% CSE $\pm$ Forskolin (10 µM), IBMX (100 µM), db-cAMP (100 µM), and olodaterol (100 nM). **c** Quantification of normalized alveolar type organoids treated with 5% CSE $\pm$ Forskolin (10 µM), IBMX (100 µM), db-cAMP (100 µM),

615   and olodaterol (100 nM). **d** Quantification of average length (diameter) of alveolar type organoids

616   (median value) treated with 5% CSE ± Forskolin (10 μM), IBMX (100 μM), db-cAMP (100 μM), and

617   olodaterol (100 nM). Data are presented as median ± SEM. **p < 0.05, **p < 0.01, ***p < 0.001, ****p

618   < 0.0001

619

620

621
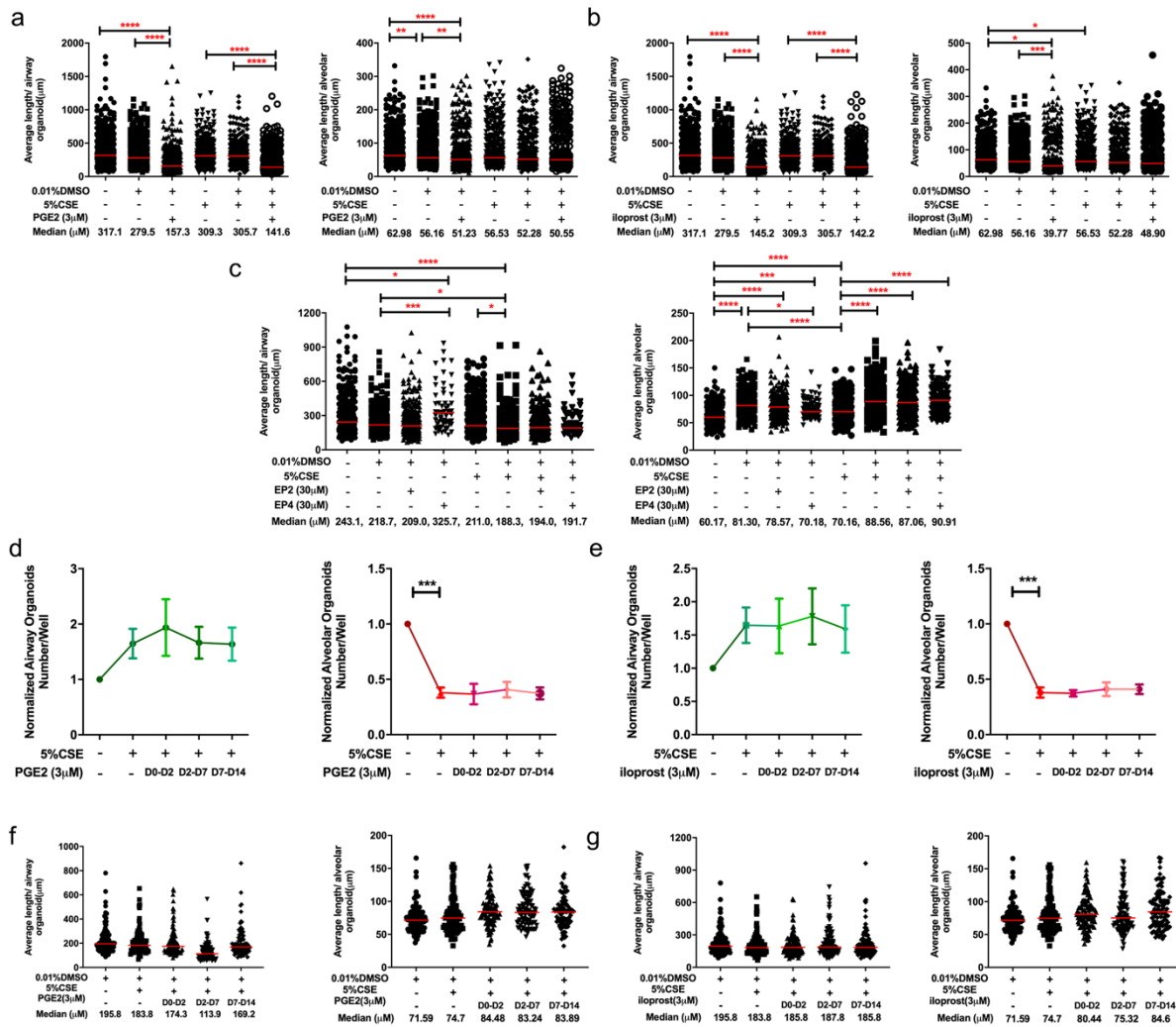
Supplementary figure 5 Quantification of lung organoid numbers and sizes in the study of PGE2/PGI2/EP2/EP4. a-b Quantification of average length (diameter) of organoids (median value) of airway and alveolar type organoids treated with 5% CSE ± PGE2 agonist (a)/iloprost (b) measured on day 14. N = 5 experiments, n > 334 organoids/group. Data are presented as median ± SEM. **c** Quantification of average length (diameter) of airway and alveolar type organoids (median value) treated with 5% CSE ± EP2/EP4 agonists measured on day 14. N = 5 experiments, n > 264 organoids/group. Data are presented as median ± SEM. **d-e** Quantification of normalized number of airway and alveolar type organoids treated with vehicle control, 5% CSE ± PGE2 agonist (d)/ iloprost (e) from day 0-2, day 2-7, or day 7-14. **f-g** Quantification of average length (diameter) of airway and alveolar type organoids (median value) treated with 5% CSE ± PGE2 agonist (f)/ iloprost (g) from day

632   0-2, day 2-7, and day 7-14. N = 2 experiments, n > 85 organoids/group. Data are presented as median

633   ± SEM.

634
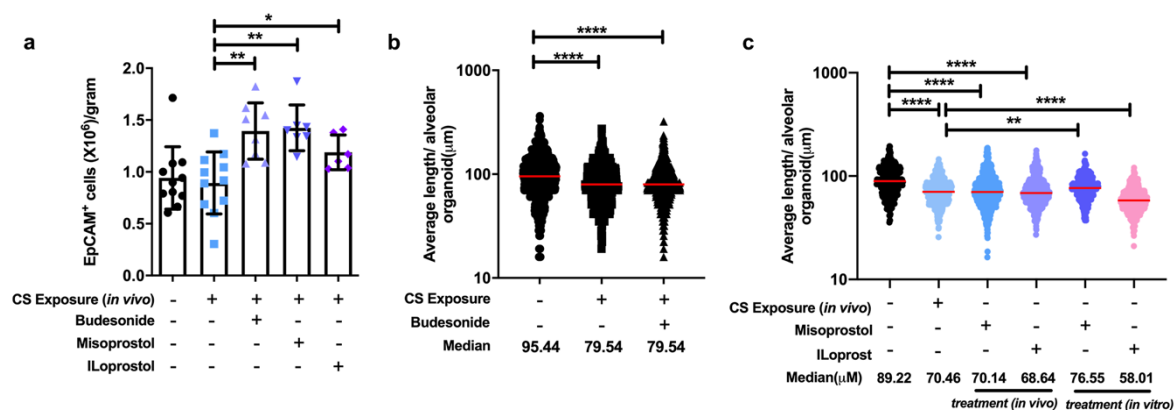
635   **Supplementary figure 6 Quantification analysis of lung organoid assay in the *in vivo* study of**

636   **PGE2/PGI2/Budesonide. a** Yield efficiency of EpCAM+ cells from mice with different treatments. **b**

637   Quantification of average length of alveolar type organoids co-cultured from CCL-206 and EpCAM+

638   cells isolated from air- (control) or CS-exposed mice with or without *in vivo* treatment with misoprostol

639   or iloprost (i.p injection). N = 4-8 experiments, n = 400 organoids/group. **c** Quantification of average

640   length of alveolar type organoids co-cultured from CCL-206 and EpCAM+ cells isolated from air- or CS-

641   exposed mice. Organoids were treated *in vitro* with misoprostol or iloprost for 14 days. N = 4-8

642   experiments, n = 400 organoids/group. Data are presented as median ± SEM. **p < 0.05, **p < 0.01,

643   ***p < 0.001, ****p < 0.0001.

644

645

References

646   1.   Kokturk, N., Yıldırım, F., Gülhan, P. Y. & Oh, Y. M. Stem cell therapy in chronic

648   obstructive pulmonary disease. How far is it to the clinic? *Am. J. Stem Cells* **7**,

649   56–71 (2018).

650   2.   Basil, M. C. *et al.* The Cellular and Physiological Basis for Lung Repair and

651   Regeneration: Past, Present, and Future. *Cell Stem Cell* **26**, 482–502 (2020).

652   3.   Volckaert, T. *et al.* Fgf10-Hippo Epithelial-Mesenchymal Crosstalk Maintains

653   and Recruits Lung Basal Stem Cells. *Dev. Cell* **43**, 48-59.e5 (2017).

654   4.   Hu, Y. *et al.* Wnt/β-catenin signaling is critical for regenerative potential of

655   distal lung epithelial progenitor cells in homeostasis and emphysema. *Stem*

656   *Cells* **38** (11) 1467-1478 (2020).

657   5.   Conlon, T. M. *et al.* Inhibition of LTβR signalling activates WNT-induced

658   regeneration in lung. *Nature* **588**, 151–156 (2020).

659   6.   Wu *et al.* Mesenchymal WNT-5A/5B Signaling Represses Lung Alveolar

660   Epithelial Progenitors. *Cells* **8** (10), 1147 (2019).

661   7.   Brandsma, C. A. *et al.* A large lung gene expression study identifying fibulin-5

662   as a novel player in tissue repair in COPD. *Thorax* **70**, 21–32 (2015).

663   8.   Kistemaker, L. E. M. *et al.* Muscarinic M3 receptors on structural cells regulate

664   cigarette smoke-induced neutrophilic airway inflammation in mice. *Am. J.*

665   *Physiol. - Lung Cell. Mol. Physiol.* **308**, L96–L103 (2015).

666   9.   Ng-Blichfeldt, J. P. *et al.* Retinoic acid signaling balances adult distal lung

667   epithelial progenitor cell growth and differentiation. *EBioMedicine 36, 461-474*

668   (2018).

669   10.   Woodby, B. *et al.* The PDE4 inhibitor CHF6001 affects keratinocyte

670   proliferation via cellular redox pathways. *Arch. Biochem. Biophys.* **685**, 1–8

(2020).

11. Zuo, H. *et al.* Cigarette smoke up-regulates PDE3 and PDE4 to decrease cAMP in airway cells. *Br. J. Pharmacol.* **175**, 2988–3006 (2018).

12. Kothe, T. B. *et al.* Surfactant and budesonide for respiratory distress syndrome: an observational study. *Pediatr. Res.* **87**, 940–945 (2020).

13. Ricci, F. *et al.* In vitro and in vivo characterization of poractant alfa supplemented with budesonide for safe and effective intratracheal administration. *Pediatr. Res.* **82**, 1056–1063 (2017).

14. Tashkin, D. P., Lipworth, B. & Brattsand, R. Benefit:Risk Profile of Budesonide in Obstructive Airways Disease. *Drugs* **79**, 1757–1775 (2019).

15. Waters, R. C. & Hochhaus, G. Characterization of a dextran-budesonide prodrug for inhalation therapy. *Eur. J. Pharm. Sci.* **129**, 58–67 (2019).

16. Shen, W. *et al.* SR9009 induces a REV-ERB dependent anti-small-cell lung cancer effect through inhibition of autophagy. *Theranostics* **10**, 4466–4480 (2020).

17. Durrington, H. J. *et al.* Circadian asthma airway responses are gated by REV-ERBα. *Eur. Respir. J.* **56**, 1–13 (2020).

18. Sundar, I. K., Rashid, K., Sellix, M. T. & Rahman, I. The nuclear receptor and clock gene REV-ERBα regulates cigarette smoke-induced lung inflammation. *Biochem. Biophys. Res. Commun.* **493**, 1390–1395 (2017).

19. Gindele, J. A. *et al.* Intermittent exposure to whole cigarette smoke alters the differentiation of primary small airway epithelial cells in the air-liquid interface culture. *Sci. Rep.* **10**, 1–17 (2020).

20. Munir, R., Lisec, J., Swinnen, J. V. & Zaidi, N. Lipid metabolism in cancer cells under metabolic stress. *Br. J. Cancer* **120**, 1090–1098 (2019).

696   21.   Gao, X. *et al.* Acetate functions as an epigenetic metabolite to promote lipid

697   synthesis under hypoxia. *Nat. Commun.* **7**, (2016).

698   22.   Whyte, M. P. *et al.* Hypophosphatemic osteosclerosis, hyperostosis, and

699   enthesopathy associated with novel homozygous mutations of DMP1 encoding

700   dentin matrix protein 1 and SPP1 encoding osteopontin: The first digenic

701   SIBLING protein osteopathy? *Bone* **132**, 115190 (2020).

702   23.   Shintani, S. *et al.* Identification and characterization of integrin-binding

703   sialoprotein (IBSP) genes in reptile and amphibian. *Gene* **424**, 11–17 (2008).

704   24.   Zhang, L. *et al.* Predictive significance of bone sialoprotein and osteopontin for

705   bone metastases in resected Chinese non-small-cell lung cancer patients: A

706   large cohort retrospective study. *Lung Cancer* **67**, 114–119 (2010).

707   25.   Guo, X. *et al.* Leptin signaling in intestinal epithelium mediates resistance to

708   enteric infection by Entamoeba histolytica. *Mucosal Immunol.* **4**, 294–303

709   (2011).

710   26.   Daniel E Shumer, N. J. N. N. P. S. Leptin receptor polymorphisms and lung

711   function decline in COPD. *Physiol. Behav.* **176**, 139–148 (2017).

712   27.   Lee, K., Lee, S. H. & Kim, T. H. The biology of prostaglandins and their role as

713   a target for allergic airway disease therapy. *Int. J. Mol. Sci.* **21**, (2020).

714   28.   Take, Y., Koizumi, S. & Nagahisa, A. Prostaglandin E Receptor 4 Antagonist in

715   Cancer Immunotherapy: Mechanisms of Action. *Front. Immunol.* **11**, 1–7

716   (2020).

717   29.   Dey, I., Lejeune, M. & Chadee, K. Prostaglandin E 2 receptor distribution and

718   function in the gastrointestinal tract. *Br. J. Pharmacol.* **149**, 611–623 (2006).

719   30.   Markovič, T., Jakopin, Ž., Dolenc, M. S. & Mlinarič-Raščan, I. Structural

720   features of subtype-selective EP receptor modulators. *Drug Discov. Today* **22**,

721   57–71 (2017).

722   31.   Nunez, F. J. *et al.* Agonist-specific desensitization of PGE2-stimulated cAMP

723   signaling due to upregulated phosphodiesterase expression in human lung

724   fibroblasts. *Naunyn. Schmiedebergs. Arch. Pharmacol.* **393**, 843–856 (2020).

725   32.   Tilley, S. L. *et al.* Receptors and pathways mediating the effects of

726   prostaglandin E2 on airway tone. *Am. J. Physiol. - Lung Cell. Mol. Physiol.*

727   **284**, 599–606 (2003).

728   33.   Buckley, J. *et al.* EP4 receptor as a new target for bronchodilator therapy.

729   *Thorax* **66**, 1029–1035 (2011).

730   34.   Birrell, M. A. *et al.* Anti-inflammatory effects of PGE2 in the lung: Role of the

731   EP4 receptor subtype. *Thorax* **70**, 740–747 (2015).

732   35.   Wang, L. *et al.* Hemodynamic and gas exchange effects of inhaled iloprost in

733   patients with COPD and pulmonary hypertension. *Int. J. COPD* **12**, 3353–3360

734   (2017).

735   36.   Zhu, Y. *et al.* A prostacyclin analogue, iloprost, protects from bleomycin-

736   induced pulmonary fibrosis in mice. *Respir. Res.* **11**, 1–12 (2010).

737   37.   Gohrbandt, B. *et al.* Iloprost to improve surfactant function in porcine

738   pulmonary grafts stored for twenty-four hours in low-potassium dextran

739   solution. *J. Thorac. Cardiovasc. Surg.* **129**, 80–86 (2005).

740   38.   Kim, N. *et al.* Effects of Inhaled Iloprost on Lung Mechanics and Myocardial

741   Function During One-Lung Ventilation in Chronic Obstructive Pulmonary

742   Disease Patients Combined With Poor Lung Oxygenation. *Anesth. Analg.* **130**

743   (5), 1407-1414 (2020).

744   39.   Lee, S. H. *et al.* Effects of intraoperative inhaled iloprost on primary graft

745   dysfunction after lung transplantation: A retrospective single center study.

746   *Med.* **95** (27), (2016).

747   40.   Gallardo, A. *et al.* The molecular clock protein Bmal1 regulates cell

748   differentiation in mouse embryonic stem cells. *Life Sci. alliance* **3**, 1–12 (2020).

749   41.   Almeida, S., Chaves, M. & Delaunay, F. Transcription-based circadian

750   mechanism controls the duration of molecular clock states in response to

751   signaling inputs. *J. Theor. Biol.* **484**, 1–11 (2020).

752   42.   Braghiroli, A. *et al.* Day and night control of copd and role of pharmacotherapy:

753   A review. *Int. J. COPD* **15**, 1269–1285 (2020).

754   43.   Zou, X. *et al.* A Systems Biology Approach Identifies Hidden Regulatory

755   Connections Between the Circadian and Cell-Cycle Checkpoints. *Front.*

756   *Physiol.* **11**, 1–9 (2020).

757   44.   Gaucher, J., Montellier, E. & Sassone-Corsi, P. Molecular Cogs: Interplay

758   between Circadian Clock and Cell Cycle. *Trends Cell Biol.* **28**, 368–379

759   (2018).

760   45.   Rahman, I. Antioxidant therapies in COPD. *Int. J. Chron. Obstruct. Pulmon.*

761   *Dis.* **1**, 15–29 (2006).

762   46.   Yu, D. *et al.* Rev-erbα can regulate the NF-κB/NALP3 pathway to modulate

763   lipopolysaccharide-induced acute lung injury and inflammation. *Int.*

764   *Immunopharmacol.* **73**, 312–320 (2019).

765   47.   Wiman, K. G. & Zhivotovsky, B. Understanding cell cycle and cell death

766   regulation provides novel weapons against human diseases. *J. Intern. Med.*

767   **281**, 483–495 (2017).

768   48.   Maddika, S. *et al.* Cell survival, cell death and cell cycle pathways are

769   interconnected: Implications for cancer therapy. *Drug Resist. Updat.* **10**, 13–29

770   (2007).

771   49.   Padgett, J. & Santos, S. D. M. From clocks to dominoes: lessons on cell cycle

772   remodelling from embryonic stem cells. *FEBS Lett.* **594**, 2031–2045 (2020).

773   50.   Farshadi, E., van der Horst, G. T. J. & Chaves, I. Molecular Links between the

774   Circadian Clock and the Cell Cycle. *J. Mol. Biol.* 3515–3524 (2020).

775   51.   Zepp, J. A. & Morrisey, E. E. Cellular crosstalk in the development and

776   regeneration of the respiratory system. *Nat. Rev. Mol. Cell Biol.* **20**, 551–566

777   (2019).

778   52.   Almeida, S., Chaves, M. & Delaunay, F. Control of synchronization ratios in

779   clock/cell cycle coupling by growth factors and glucocorticoids. *R. Soc. Open*

780   *Sci.* **7**, (2020).

781   53.   Abraham, U. *et al.* Coupling governs entrainment range of circadian clocks.

782   *Mol. Syst. Biol.* **6**, 1–13 (2010).

783   54.   Kistemaker, L. E. M. *et al.* Tiotropium attenuates IL-13-induced goblet cell

784   metaplasia of human airway epithelial cells. *Thorax* **70**, 668–676 (2015).

785   55.   Morrow, J. D. *et al.* Functional interactors of three genome-wide association

786   study genes are differentially expressed in severe chronic obstructive

787   pulmonary disease lung tissue. *Sci. Rep.* **7**, 1–11 (2017).

788   56.   Ng-Blichfeldt, J. P. *et al.* Tgf-β activation impairs fibroblast ability to support

789   adult lung epithelial progenitor cell organoid formation. *Am. J. Physiol. - Lung*

790   *Cell. Mol. Physiol.* **317** (1), L14-L28, (2019).

791   57.   Torre, D., Lachmann, A. & Ma'ayan, A. BioJupies: Automated Generation of

792   Interactive Notebooks for RNA-Seq Data Analysis in the Cloud. *Cell Syst.* **7**,

793   556-561.e3 (2018).

794